A universal velocity transformation for boundary layers with pressure gradients

By Xiang I. A. Yang, † Peng E. S. Chen, ‡ Wen Wu ¶ AND Kevin P. Griffin

The canonical law of the wall does not capture the scaling of the mean flow when a boundary layer is subjected to a strong pressure gradient. In such a boundary layer, the mean flow is affected by the spatio-temporal history of the imposed pressure gradient, and accounting for history effects remains a challenge. This work aims to address this challenge. We derive a velocity transformation that accounts for the history effects and maps the mean flow to the canonical law of the wall. The transformation is tested against channel flow with a suddenly imposed adverse or favorable pressure gradient and boundary layer flow subjected to an adverse pressure gradient. We find that the transformed velocity profiles closely follow the equilibrium law of the wall.

1. Introduction

Boundary layers with adverse pressure gradients (APGs) are common in fluid engineering. We begin our discussion by estimating the APG encountered in engineering flows. Consider, e.g., the boundary layer on the suction side of an airfoil (a control surface on a vehicle, a turbine blade, etc.). At large angles of attack, the pressure gradient causes an appreciable change in the fluid velocity. An order-of-magnitude estimate of the pressure gradient is $dP/dx = \alpha\rho U_0^2/c$, where U_0 is the velocity of the incoming fluid, c is the chord length, and α is a function of chord length, the radius of the leading edge, the attack angle, etc., and is $\sim O(0.1)$. Define $\Pi \equiv (\delta/\tau_w)\ (dP/dx)$, where δ is the boundary layer thickness, and τ_w is the wall-shear stress. We have $\Pi = \delta/\tau_w\ \alpha\rho U_0^2/c = 2\alpha(\delta/c)/C_f$. A rough estimate is: $C_f \sim O(10^{-4} - 10^{-3})$, $\alpha\delta/c \sim O(0.001 - 0.01)$ (Anderson 2011), which leads to $\Pi \sim O(1)$ to $O(100)$. Following this estimate, we consider $|\Pi|$ between 1 and 100.

The focus of the paper is the scaling of the mean flow. The canonical law of the wall (LoW) provides a good working approximation of the mean flow in a zero-pressure-gradient (ZPG) boundary layer. The LoW asserts that for $\nu/u_\tau \ll y \ll \delta$,

$$U^+ = \frac{1}{\kappa}\log(y^+) + B, \tag{1.1}$$

where ν is the kinematic viscosity, u_τ is the friction velocity, y is the wall-normal coordinate, δ is an outer length scale (boundary-layer height, half-channel height, pipe radius), U is the mean flow, the superscript + denotes normalization by the wall units, $\kappa \approx 0.4$ is the von Karman constant (keeping only one significant digit), and $B \approx 5$ is a constant (Kim et al. 1987; Marusic et al. 2013). Equation (1.1) fails when the boundary layer is subjected to a strong pressure gradient. For illustrative purposes, we consider the model

† Department of Mechanical Engineering, Pennsylvania State University
‡ College of Engineering, Peking University, China
¶ Department of Mechanical Engineering, University of Mississippi

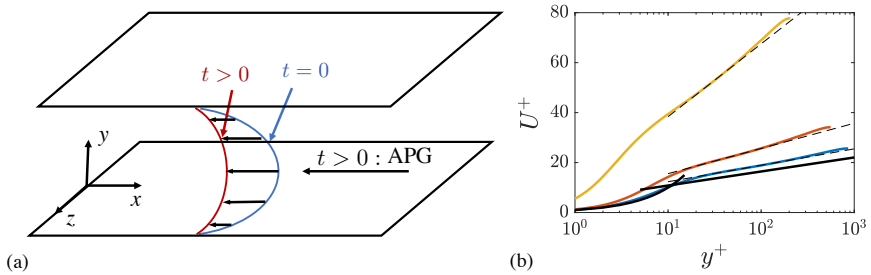

FIGURE 1. (a) Schematic of the model problem. A fully developed channel is subjected to a suddenly imposed APG and decelerates as a result. (b) Mean velocity profiles. The flow is initially at a Reynolds number $Re_\tau = 1000$. An APG $\Pi = +100$ is imposed. Shown here are velocity profiles at $tu_{\tau,0}/\delta = 0.005$ (blue), 0.035 (red), and 0.065 (yellow). The dashed lines correspond to Eq. (1.1), but we allow κ and B in Eq. (1.1) to vary. Best fits yield $\kappa = 0.35$, 0.23, 0.079, and $B = 5.8$, 5.48, 9.2 at $tu_{\tau,0}/\delta = 0.005$, 0.035, and 0.065, respectively.

problem sketched in Figure 1(a), where a fully developed channel is subjected to a suddenly imposed APG. Figure 1(b) shows the velocity profiles at a few time instants after an APG $\Pi = 100$ is suddenly imposed on a $Re_\tau = u_{\tau,0}\delta/\nu = 1000$ channel. Aside from a significantly elevated velocity profile in the core region, the region where $U^+ = y^+$ also retreats. Define

$$\Delta p^+ \equiv \frac{\nu}{\rho u_{\tau,0}^3}\frac{dP}{dx}, \text{and } \beta \equiv \frac{\delta^*}{\rho u_{\tau,0}^2}\frac{dP}{dx}, \tag{1.2}$$

which are common non-dimensional measures of the APG. Here, β is the Clauser pressure gradient coefficient, δ^* is the displacement height, and ρ is the fluid density. Note that the Clauser parameter is the ratio of the two quantities which cause the momentum thickness to increase in a spatially developing boundary layer (in the momentum integral equation). The momentum integral equation for the channel flow is different; therefore, the Clauser parameter may not be the most relevant parameter to describe the strength of a pressure gradient in a channel flow. As such, we report both Δp^+ (Lozano-Durán et al. 2020) and β. For this model problem, $\Delta p^+ = 0.1$, and $\beta = 11.6$. We see clear history effects from Figure 1(b): The mean flow deviates further away from the canonical LoW as time increases. Such history effects were also noted by Bobke et al. (2017), Volino (2020), and Romero et al. (2022), among others. Equation (1.1) with $\kappa = 0.4$ and $B = 5$ does not fit the data, not even the lower part of the velocity profiles (Galbraith et al. 1977; Perry 1966). Nonetheless, by varying the two constants, Eq. (1.1) fits the mean flow in the inertial layer (Lee & Sung 2009; Knopp et al. 2021). Here, the inertial layer is the layer within which the outer length scale does not play a role. Tuning κ and B to fit the data reduces the modeling task to a fitting exercise, which lacks universality. The same can be said about the half-power law, where one must also adjust the constants to fit the data (Knopp et al. 2021).

This work aims to establish a universal mean flow scaling for boundary-layer flows subjected to streamwise pressure gradients. We do that by a velocity transformation. The idea has received much attention in the high-Mach literature (Huang & Coleman 1994; Trettel & Larsson 2016; Griffin et al. 2021). The goal of these transformations is to find U_m and L_m,

$$U^\star = \int_0^{U^+} \frac{1}{U_m} dU, \quad y^\star = \int_0^{y^+} \frac{1}{L_m} dy, \tag{1.3}$$

such that the transformed velocity $U^\star$ follows the LoW and is a function of $y^\star$ only

irrespective of the density variation in the flow. We share a similar goal. We want to find U_m and L_m such that the transformed velocity $U^\star$ follows the LoW and is a function of $y^\star$ only irrespective of the pressure gradient, but in this context, deviations (in U^+) from the LoW are due to streamwise pressure gradients.

The rest of the paper is organized as follows. We derive the transformation in Section 2. We then test our scaling against direct numerical simulation (DNS) data. Details of the DNS data are presented in Section 3, followed by test results in Section 4. We conclude in Section 5.

2. Velocity transformation

In this section, we derive the velocity transformation from the Navier-Stokes equation and discuss its properties.

2.1. *Assumptions*

The derivation assumes the following.

(a) Incompressibility: The flow is incompressible.

(b) Two-dimensional mean flow: Pressure gradients are applied in the streamwise direction only, and the mean flow is two-dimensional.

(c) Thin boundary layer: The velocity in the wall-normal direction is much smaller than that in the streamwise direction. This assumption limits the discussion to attached flows, i.e., before incipient separation.

(d) Equilibrium initial state: The mean flow initially conforms to the LoW.

(e) Universality: Define

$$f \equiv \frac{dU^\star}{dy^\star}(1+\nu_t^+). \tag{2.1}$$

Here, f is assumed to be only a function of $y^\star$ in the inertial layer. Since $U^\star$ is a function of $y^\star$ only, it follows from this assumption that ν_t^+ is also a function of only $y^\star$ in the inertial layer. In addition, because $f = 1$ in the inertial layer of ZPG boundary-layer flows (due to the constant stress layer assumption), the universality assumption implies that $f \equiv 1$ in all flows—in the layer where the outer length scale does not play a role.

2.2. *Governing equation*

The Reynolds-averaged streamwise momentum equation reads

$$\frac{\partial U}{\partial t} + U\frac{\partial U}{\partial x} + V\frac{\partial U}{\partial y} = -\frac{\partial P}{\partial x} + \frac{\partial \tau_{xx}}{\partial x} + \frac{\partial \tau_{xy}}{\partial y}, \tag{2.2}$$

where

$$\tau_{xx} = \nu\frac{\partial U}{\partial x} - \left\langle u'u' \right\rangle, \quad \tau_{xy} = \nu\left(\frac{\partial U}{\partial y} + \frac{\partial V}{\partial x}\right) - \left\langle u'v' \right\rangle. \tag{2.3}$$

The equation assumes incompressibility and two-dimensional mean flow. Here, uppercase letters denote mean quantities, lowercase letters denote instantaneous quantities, $'$ denotes fluctuations, x, y, and z are the streamwise, wall-normal, and spanwise directions, U, V, W or u, v, w are the velocity in the three Cartesian directions, τ is the stress, and $\langle\cdot\rangle$ denotes ensemble averaging. Invoking the thin boundary-layer assumption leads to

$$\frac{\partial V}{\partial x} \ll \frac{\partial U}{\partial y}, \quad \frac{\partial \tau_{xx}}{\partial x} \ll \frac{\partial \tau_{xy}}{\partial y}. \tag{2.4}$$

It follows from Eqs. (2.2)-(2.4) that

$$\frac{\partial U}{\partial t} + U\frac{\partial U}{\partial x} + V\frac{\partial U}{\partial y} = -\frac{\partial P}{\partial x} + \frac{\partial \tau_{xy}}{\partial y}, \tag{2.5}$$

where

$$\tau_{xy} = \nu\frac{\partial U}{\partial y} - \left\langle u'v' \right\rangle. \tag{2.6}$$

We take the y derivative of both sides of Eq. (2.5),

$$\left(\frac{\partial}{\partial t} + U\frac{\partial}{\partial x} + V\frac{\partial}{\partial y}\right)\frac{\partial U}{\partial y} + \frac{\partial U}{\partial y}\frac{\partial U}{\partial x} + \frac{\partial V}{\partial y}\frac{\partial U}{\partial y} = -\frac{\partial^2 P}{\partial x \partial y} + \frac{\partial^2 \tau_{xy}}{\partial y^2}. \tag{2.7}$$

Incompressiblity requires

$$\frac{\partial U}{\partial x} + \frac{\partial V}{\partial y} = 0, \tag{2.8}$$

and the thin boundary-layer assumption suggests

$$\frac{\partial^2 P}{\partial x \partial y} \ll \frac{\partial^2 \tau_{xy}}{\partial y^2}. \tag{2.9}$$

Equations (2.7)-(2.9) lead to

$$\frac{D}{Dt}\frac{\partial U}{\partial y} = \frac{\partial^2 \tau_{xy}}{\partial y^2}. \tag{2.10}$$

Invoking the eddy viscosity ν_t, the shear stress term is

$$\tau_{xy} = \nu\frac{\partial U}{\partial y}\left(1 + \nu_t^+\right). \tag{2.11}$$

Here, ν_t is unspecified. Therefore, invoking ν_t introduces no modeling error. Plugging Eq. (1.3) into Eq. (2.11), we have

$$\frac{\nu}{\tau_{xy}}\frac{U_m}{L_m}f = 1. \tag{2.12}$$

2.3. *Transformation*

Equation (2.1) directly leads to

$$U^\star = \int_0^{y^\star} \frac{f}{1+\nu_t^+} dy^\star. \tag{2.13}$$

Equation (2.13) is a velocity transformation, but it requires knowledge of $y^\star$. In the following, we derive a transformation that maps y^+ to $y^\star$.

Integrating Eq. (2.10) in (Lagrangian) time, we have

$$\frac{\partial U}{\partial y} = \left(\frac{\partial U}{\partial y}\right)_0 + \int_0^t \frac{\partial^2 \tau_{xy}}{\partial y^2} Dt, \tag{2.14}$$

where the subscript 0 denotes quantities evaluated at $t = 0$. Note that the integration is with respect to the material differential. Invoking the assumed initial condition, the mean flow at $t = 0$ abides by the LoW; therefore,

$$\left(\frac{\partial U}{\partial y}\right)_0 = \left(\frac{u_\tau^2}{\nu}\frac{1}{F(y^+)}\right)_0. \tag{2.15}$$

Here,

$$F(\phi) = 1 + \kappa\phi\left(1 - \exp(-\phi/A)\right)^2, \tag{2.16}$$

is the damping function (Kawai & Larsson 2012), where ϕ is a dummy variable, and $A = 17$ is the van Driest damping coefficient (Cabot & Moin 2000). Invoking Eq. (2.12) and considering that $U^\star$ follows the LoW, the left-hand side of Eq. (2.14) is

$$\frac{\partial U}{\partial y} = \frac{\tau_{xy}}{\nu f}\frac{1}{F(y^\star)}. \tag{2.17}$$

Substituting Eq. (2.17) into Eq. (2.14) and rearranging, we have

$$F(y^\star) = \frac{1}{\left(\dfrac{\partial U}{\partial y}\right)_0 + \displaystyle\int_0^t \frac{\partial^2 \tau_{xy}}{\partial y^2} Dt}\frac{\tau_{xy}}{\nu f}. \tag{2.18}$$

Here, F is given in Eq. (2.16), $f \equiv 1$ for $y \ll \delta$, its value in the outer layer can be measured from an equilibrium flow (as a function of y/δ), and the derivative $(\partial U/\partial y)_0$ is known from the equilibrium LoW. Thus, $y^\star$ can be solved iteratively from Eq. (2.18).

2.4. *Discussion*

The velocity and length scale transformations are given by Eqs. (2.13) and (2.18). We have the following remarks. First, the transformation accounts for history effects through the time integral. It is interesting to note that the flow does not forget. In other words, an event at $t = 0$ and an event at a later time instant contribute equally to the transformation. Second, the transformation is valid in and outside the inertial layer. The function f is 1 in the inertial layer and varies as a function of y/δ outside. By measuring f from the initial condition as a function of y/δ, the transformation should collapse, at least in principle. Therefore, the transformation avoids the constant stress layer assumption, at least formally. Third, the transformation is descriptive rather than predictive. Closures for τ_{xy} and ν_t^+ are needed for the transformation to be predictive, a topic we do not discuss here. Fourthly, the transformation is not explicit, and one must solve $F(y^\star) = \text{Const}$ to get $y^\star$. This is rather straightforward and usually requires only a few Newton-Raphson iterations.

In the following, we simplify and write the transformation for the log layer in a ZPG boundary layer, a channel with a suddenly imposed streamwise pressure gradient, and spatially developing boundary layers with streamwise pressure gradients. First, for the log and the viscous layers in a ZPG boundary layer, we have

$$\tau_{xy} = \text{Const}. \tag{2.19}$$

We can easily verify that $U^\star = U^+$ and $y^\star = y^+$. Second, we consider Couette-Poiseuille flow. The flow is subjected to an APG near one wall and a favorable pressure gradient (FPG) near the other. The stress τ_{xy} is a linear function of y. The function f can be measured from the Couette flow, and $f = 1$. It follows that Eq. (2.18) becomes

$$F(y^\star) = \tau_{xy}^+ F(y^+). \tag{2.20}$$

Third, for a channel with a suddenly imposed streamwise pressure gradient, the mean advection is 0; therefore, the Lagrangian integration degenerates to an Eulerian one. That is, $Dt = dt$. Furthermore, measuring f from the initial condition, we have $f = 1 - y/h$. It follows that Eq. (2.18) becomes

$$F(y^\star) = \frac{1}{\left(\dfrac{\partial U}{\partial y}\right)_0 + \displaystyle\int_0^t \frac{\partial^2 \tau_{xy}}{\partial y^2} dt}\frac{\tau_{xy}}{\nu(1 - y/h)}. \tag{2.21}$$

Fourth, for a spatially developing turbulent boundary layer with streamwise pressure

Case	$Re_{\tau,0}$	Π_0	$L_x \times L_y \times L_z$	$n_x \times n_y \times n_z$	$\Delta x^+ \times \Delta y^+ \times \Delta_z^+$	N
R5A1	544	1	$4\pi \times 2 \times 2\pi$	$576 \times 243 \times 540$	$11.8 \times (0.048, 7.23) \times 6.32$	3
R5A10	544	10	$4\pi \times 2 \times 2\pi$	$576 \times 243 \times 540$	$11.8 \times (0.048, 7.23) \times 6.32$	4
R5A100	544	100	$4\pi \times 2 \times 2\pi$	$576 \times 243 \times 540$	$11.8 \times (0.048, 7.23) \times 6.32$	12
R5F10	544	-10	$4\pi \times 2 \times 2\pi$	$1024 \times 512 \times 1024$	$13.4 \times (0.13, 6.72) \times 6.70$	1
R5F100	544	-100	$4\pi \times 2 \times 2\pi$	$1024 \times 512 \times 1024$	$12.6 \times (0.12, 6.32) \times 6.29$	1
R10A10	1000	10	$8\pi \times 2 \times 3\pi$	$2048 \times 512 \times 1536$	$12.3 \times (0.12, 6.15) \times 6.13$	2
R10A100	1000	100	$8\pi \times 2 \times 3\pi$	$2048 \times 512 \times 1536$	$12.3 \times (0.12, 6.15) \times 6.13$	3

TABLE 1. DNS details of channel flows subjected to a suddenly imposed adverse ($\Pi > 0$) or favorable ($\Pi < 0$) pressure gradient. $Re_{\tau,0}$ is the initial Reynolds number. Π is positive for APG and negative for FPG. L_x, L_y, and L_z are the domain sizes in the streamwise, wall-normal, and spanwise directions. Here, normalization is by the half-channel height. n_x, n_y, and n_z are the number of grid points in the three Cartesian directions. Δx^+, Δy^+, and Δz^+ are the grid spacings in the three directions. For Δy^+, we list the resolution at the wall and the channel center. Here, we list the grid resolution at the beginning or the end of the DNSs. For $\Pi > 0$, a finer grid must be employed at the beginning than at the end, and we list the grid resolution at the beginning of the DNS and vice versa. N is the number of ensembles used to compute the flow statistics.

gradients, Lagrangian integration is along the streamline, and Eq. (2.18) becomes

$$F(y^\star) = \frac{1}{\left(\dfrac{\partial U}{\partial y}\right)_0 + \displaystyle\int_0^s \frac{\partial^2 \tau_{xy}}{\partial y^2} \frac{ds}{|\mathbf{U}|}} \frac{\tau_{xy}}{\nu f}, \tag{2.22}$$

where ds is along a streamline, and $|\mathbf{U}|$ is the velocity magnitude.

3. Data

To test the velocity transformation, we conduct DNSs of channel subjected to a suddenly imposed APG or FPG. The flow is sketched in Figure 1(a). Table 1 shows the DNS details. The nomenclature is as follows: R[Re_τ/100]F/A[|Π|], where F is for FPG, and A is for APG. For APGs, Π is 1, 10, or 100, corresponding to a weak APG, a moderate APG, and a strong APG. For FPGs, $\Pi = -10$ or -100, corresponding to a moderate and a strong FPG. Note that FPGs are not very challenging (or interesting) in this context because the canonical LoW works fairly well for flows with FPGs (Townsend 1956; Mellor & Gibson 1966). The initial Reynolds number is $Re_{\tau,0} = 544$ or 1000. The Reynolds number increases when an FPG is applied and decreases when an APG is applied. The size of the channel is $(4\pi \times 2 \times 2\pi)\delta$ for the R5 ($Re_\tau = 544$) cases and $(8\pi \times 2 \times 3\pi)\delta$ for the R10 ($Re_\tau = 1000$) cases. The domain sizes are larger than that of the minimal channel (Lozano-Durán & Jiménez 2014). The grid resolution is comparable to that of Mathur et al. (2018) and Yang et al. (2021) and is such that the flow is well resolved from the beginning to the end. We employ statistically uncorrelated initial flow fields and repeat the simulations multiple times to get converged statistics following Lozano-Durán et al. (2020). The code we use is the same as the one used by Lee & Moser (2015). Details of the code are presented by Graham et al. (2016) and Lee & Moser (2015) and are not detailed here for brevity.

We also use the boundary-layer data from Bobke et al. (2017). The flows are sketched in Figure 2. Flow parameters that are relevant to this analysis are listed in Table 2. Further details are not shown for brevity.

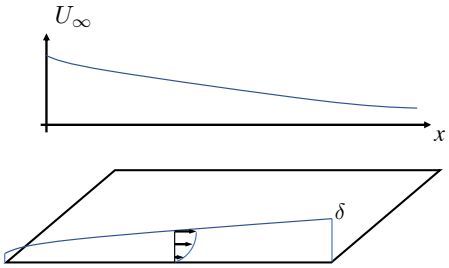

FIGURE 2. A sketch of a boundary layer subjected to APGs. The pressure gradient is imposed by varying the freestream velocity. The reader is directed to Bobke et al. (2017) for more details.

Case	Flow type	Ref.	Re_τ	Π
m13	APG-BL	Bobke et al. (2017)	[190; 896]	[3.80; 5.51]
m16	APG-BL	Bobke et al. (2017)	[189; 934]	[5.82; 8.67]
m18	APG-BL	Bobke et al. (2017)	[192; 973]	[7.29; 12.5]
b1	APG-BL	Bobke et al. (2017)	[190; 862]	≈ 4.11
b2	APG-BL	Bobke et al. (2017)	[189; 910]	≈ 7.55
ZPG	ZPG-BL	Schlatter & Örlü (2010)	[252; 1271]	0

TABLE 2. Details of the boundary-layer flows. The nomenclature of the BL cases is the same as that used by Bobke et al. (2017). We also include the ZPG-BL data from Schlatter & Örlü (2010) as the standard case.

4. Results

First, we present the channel flow results. Figures 3 and 4 show the mean velocity profiles in the APG cases. Figure 3 shows the R5 results, and Figure 4 shows the R10 results. The results at other time instants are similar and are not shown for brevity. In R5A1, a weak APG is applied, and the flow remains in a quasi-equilibrium state. As a result, both U^+ and $U^\star$ follow the LoW. In R5A10 and R10A10, a moderate APG is applied, and we see noticeable deviations in U^+ from the LoW at $t = O(10)$. Nonetheless, $U^\star$ follows the LoW closely at all time instants. In R5A100 and R10A100, a strong APG is applied. The viscous units fail to collapse the velocity profiles, and only $U^\star$ follows the LoW. Figure 5 shows the mean velocity profiles in the two FPG cases. FPGs lead to noticeable deviations from the LoW in case R5F100, but the transformed velocity profiles collapse with the LoW. Last, Figure 6 shows the boundary-layer results. We see that the transformation collapses all profiles, and the transformed velocity profiles follow the LoW. However, the collapse is less convincing compared with the results in Figures 3 and 4. This is largely because the boundary-layer data, particularly the τ_{xy} data, suffer from a lack of statistical convergence (results not shown for brevity). Compared with channel flow, where one can average in time and in the streamwise and the spanwise directions, one can average a boundary-layer flow only in time and in the spanwise direction.

5. Conclusions

We derive a velocity transformation from the Navier-Stokes equation that maps the mean velocity profiles in non-equilibrium boundary layers to the LoW. This is the first time the velocity transformation idea has been applied to handle non-equilibrium effects. History effects are accounted for in the transformation through a Lagrangian integral originating in the equilibrium state. This integration weights all history events equally,

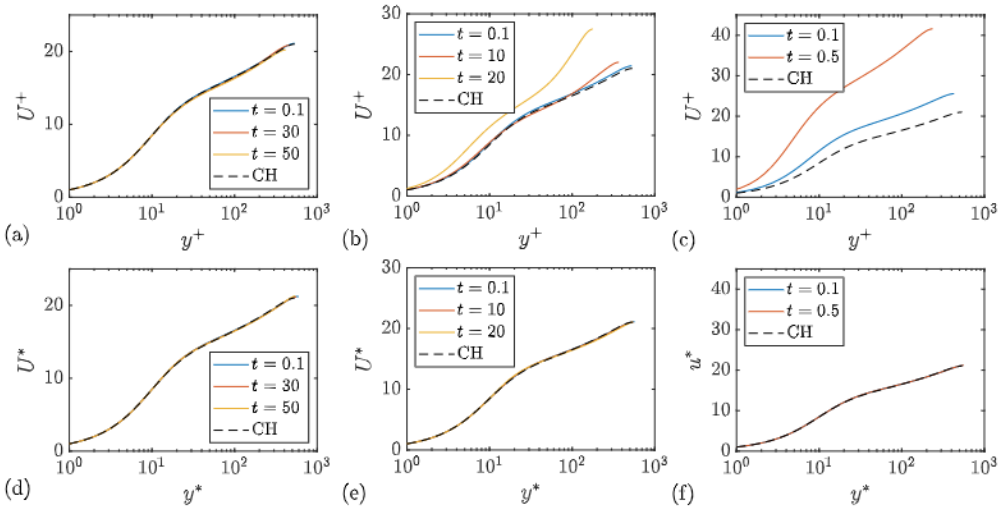

FIGURE 3. Mean velocity profiles at a few time instants. (a, b, c) U^+ as a function of y^+. (d, e, f) $U^\star$ as a function of $y^\star$. (a, d) R5A1. (b, e) R5A10. (c, f) R5A100. Here, time t is normalized with $\delta/u_{\tau,0}$. CH is the velocity profile in a fully developed $Re_\tau = 544$ channel.

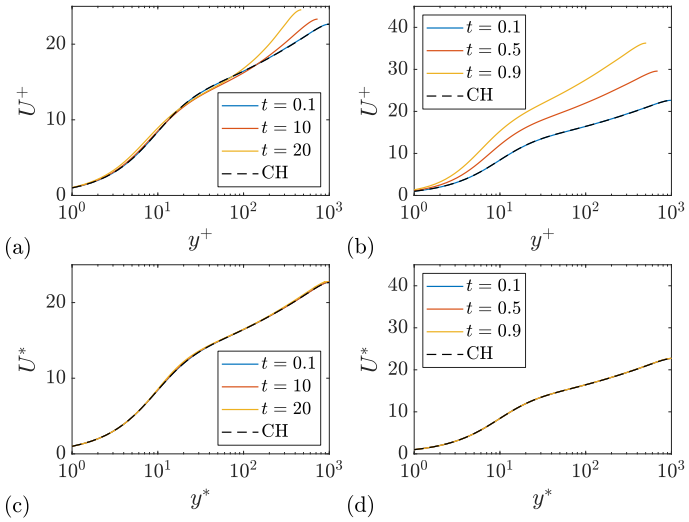

FIGURE 4. Mean velocity profiles at a few time instants. (a, b) U^+ as a function of y^+. (c, d) $U^\star$ as a function of $y^\star$. (a, c) R10A10. (b, d) R10A100. CH is the velocity profile in a fully developed $Re_\tau = 1000$ channel.

and the flow does not forget unless the effects of one event are canceled by another. The transformation is tested in channel flows subjected to suddenly imposed pressure gradients, Couette-Poiseuille flows, and spatially developing turbulent boundary layers with streamwise pressure gradients. We show that while the wall-unit scaled velocity profiles deviate from the LoW, the transformed profiles follow the LoW closely, irrespective of the pressure gradients. A limitation of the present transformation is that it is descriptive rather than predictive. Future work will focus on closing the term τ_{xy}.

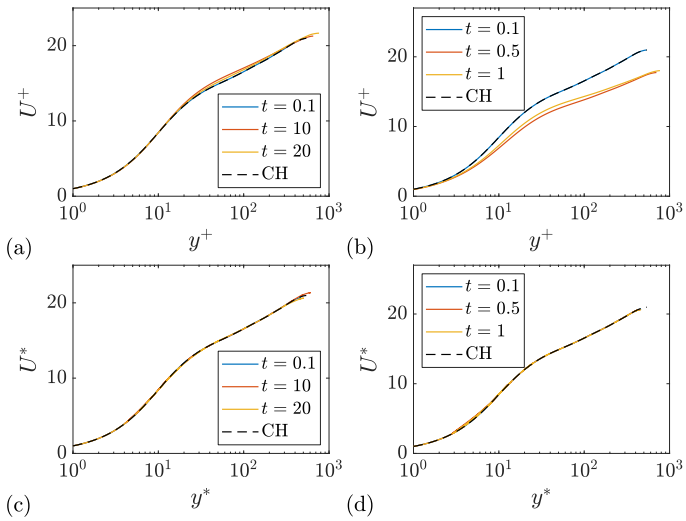

FIGURE 5. Mean velocity profiles at a few time instants. (a, b) U^+ as a function of y^+. (c, d) $U^\star$ as a function of $y^\star$. (a, c) R5F10. (b, d) R5F100. CH is the velocity profile in a fully developed $Re_\tau = 544$ channel.

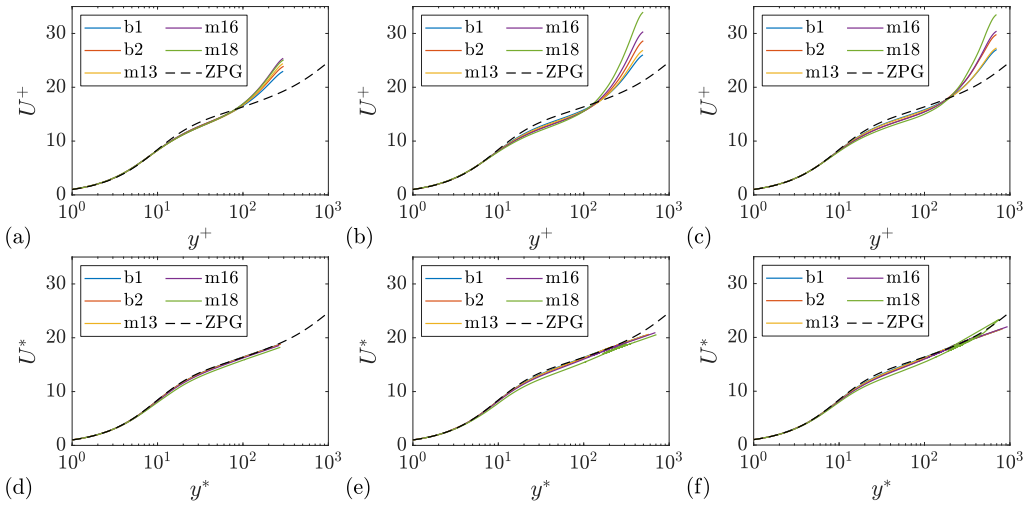

FIGURE 6. Mean velocity profiles in boundary-layer flows at multiple streamwise locations: (a) and (d) for $Re_\tau = 300$; (b) and (e) for $Re_\tau = 500$; (c) and (f) for $Re_\tau = 700$. ZPG is the velocity profile in a ZPG boundary layer at $Re_\tau = 1272$.

Acknowledgments

Yang thanks Parviz Moin, Ahmed Elnahhas, Rahul Agrawal, Adrian Lozano-Duran, Jane Bae, Olaf Marxen, Michael Cui, and Mostafa Momen for their generous help during his stay at Stanford.

REFERENCES

ANDERSON, J. 2011 *Fundamentals of Aerodynamics*. McGraw Hill.

Bobke, A., Vinuesa, R., Örlü, R. & Schlatter, P. 2017 History effects and near equilibrium in adverse-pressure-gradient turbulent boundary layers. *J. Fluid Mech.* **820**, 667–692.

Cabot, W. & Moin, P. 2000 Approximate wall boundary conditions in the large-eddy simulation of high Reynolds number flow. *Flow Turbul. Combust.* **63**, 269–291.

Galbraith, R. M., Sjolander, S. & Head, M. 1977 Mixing length in the wall region of turbulent boundary layers. *Aeronaut. Quart.* **28**, 97–110.

Graham, J., Kanov, K., Yang, X. I. A., Lee, M., Malaya, N., Lalescu, C., Burns, R., Eyink, G., Szalay, A., Moser, R. *et al.* 2016 A web services accessible database of turbulent channel flow and its use for testing a new integral wall model for LES. *J. Turbul.* **17**, 181–215.

Griffin, K. P., Fu, L. & Moin, P. 2021 Velocity transformation for compressible wall-bounded turbulent flows with and without heat transfer. *PNAS* **118**, e2111144118.

Huang, P. & Coleman, G. N. 1994 Van Driest transformation and compressible wall-bounded flows. *AIAA J* **32**, 2110–2113.

Kawai, S. & Larsson, J. 2012 Wall-modeling in large eddy simulation: length scales, grid resolution, and accuracy. *Phys. Fluids* **24**, 015105.

Kim, J., Moin, P. & Moser, R. 1987 Turbulence statistics in fully developed channel flow at low Reynolds number. *J. Fluid Mech.* **177**, 133–166.

Knopp, T., Reuther, N., Novara, M., Schanz, D., Schülein, E., Schröder, A. & Kähler, C. 2021 Experimental analysis of the log law at adverse pressure gradient. *J. Fluid Mech.* **918**, A17.

Lee, J.-H. & Sung, H. J. 2009 Structures in turbulent boundary layers subjected to adverse pressure gradients. *J. Fluid Mech.* **639**, 101–131.

Lee, M. & Moser, R. D. 2015 Direct numerical simulation of turbulent channel flow up to $Re_\tau \approx 5200$. *J. Fluid Mech.* **774**, 395–415.

Lozano-Durán, A., Giometto, M. G., Park, G. I. & Moin, P. 2020 Non-equilibrium three-dimensional boundary layers at moderate Reynolds numbers. *J. Fluid Mech.* **883**, A20.

Lozano-Durán, A. & Jiménez, J. 2014 Effect of the computational domain on direct simulations of turbulent channels up to $Re_\tau = 4200$. *Phys. Fluids* **26**, 011702.

Marusic, I., Monty, J. P., Hultmark, M. & Smits, A. J. 2013 On the logarithmic region in wall turbulence. *J. Fluid Mech.* **716**, R3.

Mathur, A., Gorji, S., He, S., Seddighi, M., Vardy, A., ODonoghue, T. & Pokrajac, D. 2018 Temporal acceleration of a turbulent channel flow. *J. Fluid Mech.* **835**, 471–490.

Mellor, G. & Gibson, D. 1966 Equilibrium turbulent boundary layers. *J. Fluid Mech.* **24**, 225–253.

Perry, A. 1966 Turbulent boundary layers in decreasing adverse pressure gradients. *J. Fluid Mech.* **26**, 481–506.

Romero, S., Zimmerman, S., Philip, J., White, C. & Klewicki, J. 2022 Properties of the inertial sublayer in adverse pressure-gradient turbulent boundary layers. *J. Fluid Mech.* **937**, A30.

Schlatter, P. & Örlü, R. 2010 Assessment of direct numerical simulation data of turbulent boundary layers. *J. Fluid Mech.* **659**, 116–126.

Townsend, A. 1956 The properties of equilibrium boundary layers. *J. Fluid Mech.* **1**, 561–573.

Trettel, A. & Larsson, J. 2016 Mean velocity scaling for compressible wall turbulence with heat transfer. *Phys. Fluids* **28**, 026102.

Volino, R. J. 2020 Non-equilibrium development in turbulent boundary layers with changing pressure gradients. *J. Fluid Mech.* **897**, A2.

Yang, X. I. A., Hong, J., Lee, M. & Huang, X. L. D. 2021 Grid resolution requirement for resolving rare and high intensity wall-shear stress events in direct numerical simulations. *Phys. Rev. Fluids* **6**, 054603.